Intermolecular interactions between hypervalent molecules: Ph_2IX and XF_3 (X = Cl, Br, I) dimers†

Gregory A. Landrum,‡[a] Norman Goldberg,§[a] Roald Hoffmann*[a] and Ruslan M. Minyaev[b]

[a] *Department of Chemistry and Materials Science Center, Cornell University, Ithaca, NY 14853-1301, USA*

[b] *Institute of Physical and Organic Chemistry, Rostov State University, 194/2 Stachka Ave., Rostov-on-Don 344090, Russian Federation*

The intermolecular bonding in dimers of the T-shaped hypervalent title compounds is analyzed using a combination of density functional calculations and qualitative arguments. Fragment molecular orbital interaction diagrams lead us to the conclusion that the bonding in these species can be understood using the language of donor-acceptor interactions: mixing between occupied states on one fragment and unoccupied states on the other. There is also a strong electrostatic contribution to the bonding. The calculated strengths of these halogen—halogen secondary interactions are all less than 10 kcal mol^{-1}. There is a very soft potential energy surface for the deformation that makes the bridge in the dimers asymmetrical.

In this contribution we take another step towards understanding the nature of secondary bonds: unusually short intermolecular interactions that, while relatively weak compared to 'normal' covalent bonds, can have a profound effect upon the crystal structures of molecules.[1–4] Our previous work, focusing on the trihalides and related systems,[5] laid the groundwork for interpreting intermolecular interactions in terms of donor-acceptor and/or electron-rich three-center (hypervalent) bonding. The idea that connects these bonding types is orbital interaction or mixing between occupied levels on one fragment and unoccupied levels on another. This is illustrated in Scheme 1.

Here one component, possessing only a donor function (ψ_D), interacts with a molecular fragment, which has both donor (ψ_A) and acceptor (ψ_A^*) functions. The net result of the interaction is a partial occupation of the previously empty ψ_A^* level, which is why we label the molecular fragment as an acceptor. The resulting orbitals sketched in this schematic representation of a donor-acceptor interaction are, of course, the familiar σ orbitals of hypervalent I_3^-, formed here from I_2 and I^-.[5,6,7]

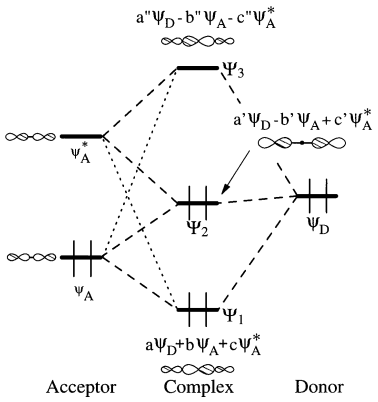

Scheme 1

† *Non-SI units employed:* kcal ≈ 4.18 J; eV ≈ 1.6 × 10^{-19} J.

‡ Current address: Institut für Anorganische Chemie, RWTH-Aachen, Prof.-Pirlet-Str. 1, D-52074 Aachen, Germany.

§ Current address: Institut für Organische Chemie, TU-Braunschweig, Hagenring 30, D-38106 Braunschweig, Germany.

While our previous work provided a simple model to use in understanding intermolecular interactions, it did not lend sufficient insight into the energetics of secondary bonding. In the trihalides and hydrogen bihalides, atomic anions and neutral molecules interact. There are strong forces at work in these systems, which arise both from electrostatics and from electron-electron repulsion (forming X_3^- from X^- and X_2 allows the negative charge on X^- to delocalize over three atoms, lessening the electron-electron repulsion considerably). Both of these factors strongly increase the bonding energy beyond what it would be between equivalent neutral species. In this work we focus on two families of compounds, which share some structural similarities and exhibit substantial intermolecular interactions between neutral closed-shell species. Closed-shell interactions in inorganic systems have been reviewed recently.[8]

The first group of compounds we will examine is the diaryliodonium halides: R_2IX. We will specifically consider the species where R = phenyl. These compounds, first crystallographically characterized by Alcock for X = Cl, Br and I in 1977,[9] form dimers in the crystal.

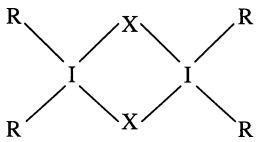

These are ideal examples of secondary bonds: the bridging I—X bonds are 0.7 Å longer than single bonds but considerably shorter than van der Waals contacts, and the R—I—X angles are close to 180°. In the crystal structures, the dimers are nearly symmetrical, with I—X distances approximately equal.

We have chosen this class of compounds for a number of reasons. First of all, hypervalent iodine is of general interest to synthetic chemists and has been extensively studied (see ref. 10, 11, and 12 for recent reviews). Secondly, the secondary bonding here does not result in the formation of an infinite network (a common occurrence); this is convenient because it allows us to use molecular tools to understand the interactions. The fact that experimental data are available for most of the halogen series (X = Cl, Br, I) allows us to explore the effects of changing the identity of the bridging X atoms.

Finally, while the system is fairly large (28 heavy atoms), it is still amenable to study with density functional theory.

The second group of compounds that we will examine are the hypervalent XF_3 interhalogens with X = Cl, Br and I. These species are known to dimerize in the liquid phase,[13–15] as shown here.

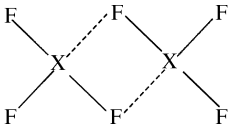

In the solid state, ClF_3 and BrF_3 form polymeric structures.[16,17] A recent review[18] summarized previous theoretical studies of XF_3 species. Here we focus on the nature of the bonding between XF_3 molecules in $[XF_3]_2$ dimers.

An analysis of these two different types of dimers of neutral, hypervalent molecules should provide us with a good feeling for the general nature and energetics of secondary bonds between halogen atoms.

The important interactions holding all of our dimers together are intermolecular halogen—halogen bonds. These have been extensively studied in previous work. A detailed analysis of the results of crystallographic database searches for intermolecular contacts involving halogens bound to carbon[19] led to the following conclusions: intermolecular contacts between electrophilic atoms and halogens occur normal to the C—X bond; contacts between nucleophilic atoms and halogens occur along the C—X bond; halogen—halogen contacts occur in an L-shaped geometry, with the C—X bond axis of one molecule normal to the C—X bond axis of the other. The intermolecular coordination geometries are sketched in Scheme 2, where E indicates an electrophile and N a nucleophile.

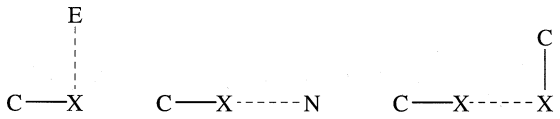

Scheme 2

The L-shaped intermolecular halogen—halogen interaction was already well-known from the gas-phase structures of HF—ClF[20] and HF—Cl_2,[21] and can also be found in the 'herringbone' pattern observed in solid X_2.[22]

In more recent analyses of intermolecular Cl—Cl, halogen—oxygen and halogen—nitrogen interactions based upon both crystallographic database searches and intermolecular perturbation theory, Stone and coworkers reach similar conclusions about the preferred orientation of these contacts.[23,24] The theoretical results lead to the conclusion that the dominant factors determining the strengths of these interactions are electrostatics and exchange repulsion. The authors attribute the preferred geometries of the interactions to asymmetries in the charge distribution around the halogen atoms. This idea of 'polar-flattening,'[25] an asymmetry in the electron density of a bound halogen atom where the electron density is more contracted parallel to the bond than perpendicular to it, has been supported in the case of solid Cl_2 by analysis of the Laplacians of both theoretical and experimental charge densities.[26]

Here we will use molecular orbital (MO)—as opposed to electron density—arguments to understand the intermolecular interactions. It is our belief that MO theory lends itself more readily to a qualitative understanding of the forces holding these species together.

Computational Methodology

The calculations were carried out using the Amsterdam Density Functional (ADF) program.[27–29] Gradient corrections for the $[Ph_2IX]_2$ systems were performed using the Becke (exchange)[30,31] and Perdew (correlation)[32,33] formulations. The valence atomic orbitals were represented using a basis set of Slater-type orbitals (STOs). Triple-ζ basis sets (three STOs per AO) with one polarization function were used for the halides. Triple-ζ basis sets with two added polarization functions were used for carbon and hydrogen.[34]

For the XF_3 dimers, the Becke exchange correction is used along with the Lee–Yang–Parr[35–37] correlation correction (this combination is known as the BLYP functional). Triple-ζ basis sets with two polarization functions were used for all atoms except I, for which a single polarization function was employed.

For both the Ph_2IX and XF_3 dimers, the core orbitals of the atoms were frozen out to: 1s (F,C), 2p (Cl), 3p (Br), and 4p (I).[27]

Relativistic effects were not included in the calculations. Our experience with computations on these types of systems indicates that inclusion of relativistic corrections has only small effects upon the calculated geometries and bonding energies.

The contour plots of molecular orbitals from ADF were generated using viewkel, a part of YAeHMOP.[38] These plots contain contributions from both the valence and core functions (which can be seen in the regions near the atomic nuclei in each plot). All MO plots use the same contour levels: −0.10 to +0.10 in 0.01 increments.

We will make heavy use of the transition-state energy decomposition procedure provided in ADF. This method, presented in detail in ref. 39, was also described from a qualitative perspective in our earlier work.[5]

Results and Discussion

The Ph_2IX monomers

We begin our discussion of the $[Ph_2IX]_2$ dimers with a detailed look at the bonding in the Ph_2I^+ cation and the corresponding Ph_2IX monomers. Ph_2I^+ is, of course, a classical cation; it is possible to draw a perfectly reasonable Lewis structure for the molecule (see Scheme 3).

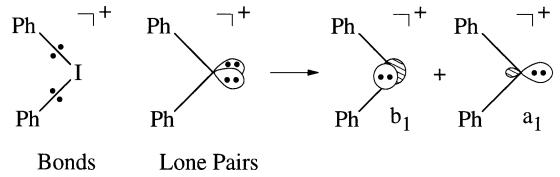

Scheme 3

By including the two lone pairs (shown in Scheme 3 along with their symmetry-adapted MO equivalents), the iodine has a complete octet and is electronically satisfied. These two lone pairs were postulated as important frontier orbitals of Ph_2I^+ in order to understand the results of Mössbauer experiments on $[Ph_2IX]_2$ species.[40]

In the C_{2v} optimized structure of Ph_2I^+, the C—I distances are 2.20 Å and the C—I—C angle is 89.5°. Two views of the optimized geometry of Ph_2I^+ are shown in Fig. 1. Note the orientation of the phenyl rings, presumably sterically determined.

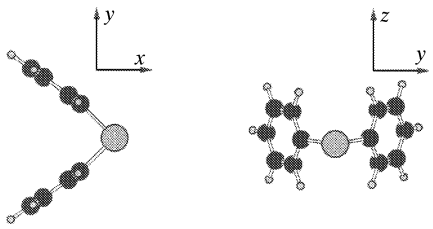

Fig. 1 Two views of the optimized structure of Ph_2I^+

The important frontier orbitals of the iodonium ion are shown in Fig. 2. The Highest Occupied Molecular Orbital (HOMO) and the two levels immediately below it in energy ($7a_2$, $10b_2$ and $8b_1$) are centered almost entirely on the phenyl rings; the iodine contributions to these orbitals are less than 1%.

Contour plots of the two lone pairs we expect to see at the iodine (see Scheme 3) are shown in Fig. 3. Contrary to what we might expect, these two lone pairs are not found in the frontier orbital region, but lie deeper in energy. In fact, they are both below the energy window shown in Fig. 2 at −11.78 ($7b_1$) and −12.34 ($11a_1$) eV.[41] The $12a_1$ has a little iodine character, but is mainly centered on the phenyls.

We now build up Ph_2IX by approaching X^- to Ph_2I^+, in the geometry shown below:

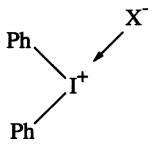

As a reviewer has suggested, the shape of the $11b_2$ LUMO suggests that an approach maximizing overlap with that orbital would be favored. Indeed, as X^- approaches Ph_2I^+, there is significant overlap between the X^- σ orbital[42] and the low-lying unoccupied $11b_2$ and $13a_1$ orbitals on Ph_2I^+. This overlap leads to formation of an I—X bond, partial occupation of the Ph—I antibonding $11b_2$ and $13a_1$ levels, and charge transfer from X^- to Ph_2I^+. Since the X^- to Ph_2I^+ charge transfer partially occupies antibonding levels of Ph_2I^+, it leads to geometrical changes in the Ph_2I^+ fragment. The most obvious of these is a lengthening of the Ph—I bond opposite to X^-. The important geometric variables for the Ph_2IX structures within the C_s point group are defined in Scheme 4. The values of these parameters for X = Cl, Br and I, as optimized in our calculations, are given in Table 1.

The geometries of the Ph_2I^+ fragment in Ph_2ICl, Ph_2IBr and Ph_2I_2 are quite similar. This is easily explained by the essentially constant amount of charge (0.56 electrons) transferred to Ph_2I^+ from X^-.[43] This is the charge transfer, into antibonding levels on the Ph_2I^+ fragment, that perturbs the Ph_2I^+ geometry.

The Ph_2I^+--X^- interaction energies are substantial: 106.2, 101.6 and 93.2 kcal mol^{-1} for X = Cl, Br and I. The energies are so large quite simply because these interactions are between anions and cations. There are huge electrostatic contributions to the bonding in these species.

The shapes of the MOs of Ph_2ICl, Ph_2IBr and Ph_2I_2 are also very similar to each other. The energy levels and some important frontier MOs of Ph_2ICl are shown in Fig. 4. The two highest occupied MOs of Ph_2ICl, 16a″ (perpendicular to the *xy* plane, not shown in Fig. 4) and 25a′ are composed almost entirely of Cl p_π orbitals. These are two of the Cl lone pairs. The LUMO of Ph_2ICl, 26a′, has its largest contribution (40%) from I. This orbital will be important in the following development; it is ideally suited to act as an acceptor orbital when we proceed to form the $[Ph_2ICl]_2$ dimer below. The expected iodine lone pairs, 20a′ and 13a″, appear at −8.95

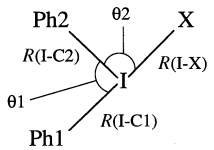

Scheme 4

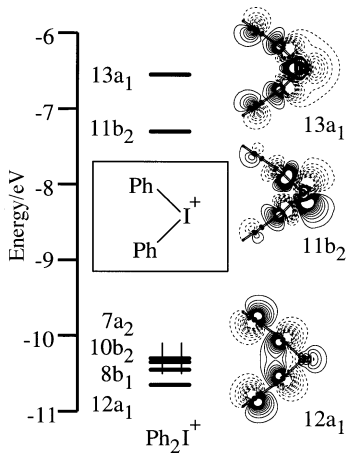

Fig. 2 Energy level diagram in the frontier orbital region for Ph_2I^+. Contour plots in the *xy* plane of the frontier orbitals with large iodine contributions are shown on the right

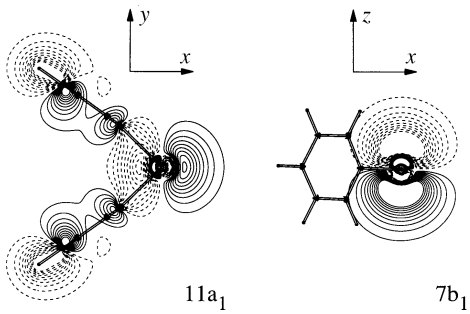

Fig. 3 Contour plots of the lone pair orbitals of Ph_2I^+. The orbitals $11a_1$ and $7b_1$ lie at −12.34 and −11.78 eV, respectively

Table 1 Geometric data for the optimized Ph_2IX species. All optimizations were carried out in the C_s symmetry. C1 and C2 refer to the carbon atoms through which Ph1 and Ph2 coordinate to I

	Ph_2ICl	Ph_2IBr	Ph_2I_2
R(I—X)/Å	2.70	2.88	3.22
R(I—C1)/Å	2.26	2.26	2.30
R(I—C2)/Å	2.20	2.20	2.20
θ1/°	80	82	82
θ2/°	87	86	88

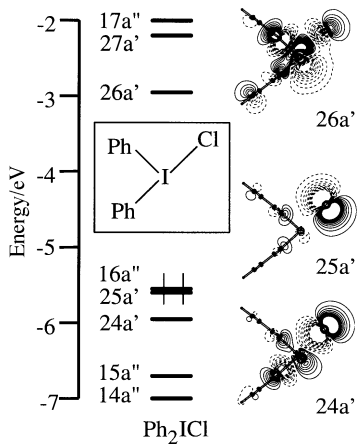

Fig. 4 Energy level diagram for the frontier orbital region of Ph_2ICl. Contour plots in the *xy* plane of the important frontier orbitals are shown on the right

and −7.82 eV, respectively, once again well outside the energy window of Fig. 4.

The central iodine in Ph_2IX has two substituents that are nearly linearly aligned. This is a situation similar to that in PF_5, SF_4, BrF_3 and XeF_2, and because of the electron count at I, it seems reasonable to assign it the label 'hypervalent'. In fact, if we take a closer look at the orbitals of Ph_2ICl, we find analogs of the important σ MOs of I_3^-, our archetypical hypervalent molecule.[5,6,44] The three relevant MOs, along with iconic representations of the corresponding orbitals from I_3^-, are shown in Fig. 5. Considering the very large differences between I_3^- and Ph_2ICl, the similarities between the orbitals are quite striking. As in I_3^-, this set of three orbitals is occupied up through the second MO (24a′ here).

The $[Ph_2IX]_2$ dimers

The experimental geometries of the $[Ph_2IX]_2$ dimers are nearly symmetrical: the I—X distances differ by at most 0.04 Å.[9] Because of this, and for reasons of computational expediency (these molecules really are quite big), the geometries of the $[Ph_2IX]_2$ dimers were optimized in the D_{2h} symmetry. In all three optimized geometries, the I—C distances are 2.22–2.23 Å and the C—I—C angles are 84–85°. The I—X distances, of course, vary quite a bit: 2.99, 3.14 and 3.44 Å for X = Cl, Br and I. These distances match those from the X-ray structures of Ph_2IX quite well: to within 0.1 Å.

There are two ways to approach an understanding of the bonding in $[Ph_2IX]_2$ species. The first is to view $[Ph_2IX]_2$ as arising from the interaction of two Ph_2IX units. The second approach, to be discussed subsequently, is to consider the dimer as being formed from two Ph_2I^+ and two X^- ions.

A Fragment Molecular Orbital (FMO) interaction diagram for the formation of $[Ph_2ICl]_2$ from two Ph_2ICl monomers is shown in Fig. 6. Note that in this FMO diagram we deviate slightly from our usual practice by only showing one of the fragments. Since both Ph_2ICl fragments are identical, no information is lost by doing this. This interaction, where the formerly unoccupied 26a′ orbital is mixed into occupied levels *via* interaction with 25a′ (in $[Ph_2ICl]_2$, the 26a′ orbital of each Ph_2ICl fragment has an occupation of 0.26 electrons), shows all the signs of donor-acceptor bonding. There is, of course, no net electron transfer between the two fragments, which are identical. The charge transfer is 'two-way': donation and acceptance are exactly balanced.

The bonding energies of the $[Ph_2IX]_2$ dimers, corrected for the preparation energies of the fragments (we will say more about this below), as well as the Transition State procedure energy decompositions,[39] are shown in Table 2. The first thing that jumps out from this table is that the bonding energy

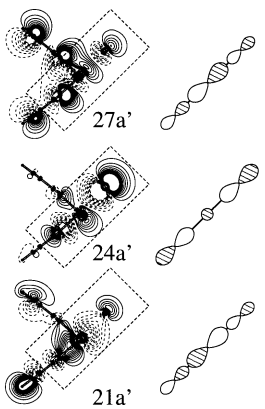

Fig. 5 The MOs of Ph_2ICl involved in electron-rich three-center bonding (left) and icons of the corresponding orbitals from I_3^- (right). To guide the eye, the three centers involved in the bonding are outlined with a dashed box

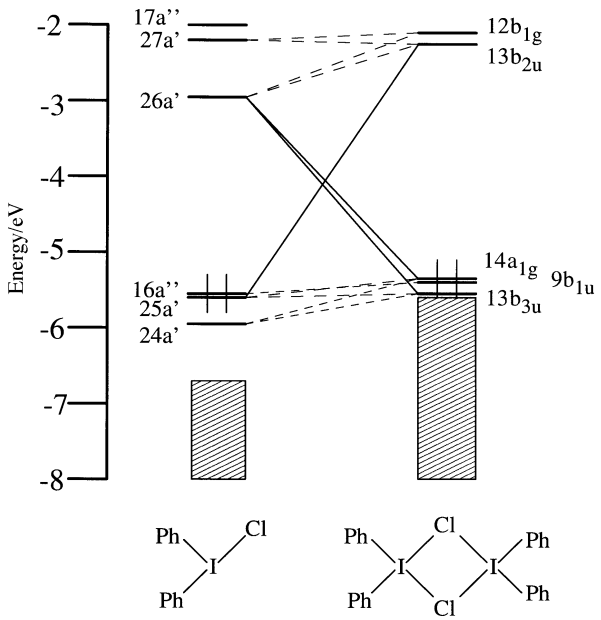

Fig. 6 Fragment Molecular Orbital (FMO) interaction diagram for the formation of $[Ph_2ICl]_2$ from two Ph_2ICl fragments. Only one of the identical Ph_2ICl fragments is included in the plot. Interactions involved in the donor-acceptor interaction are highlighted with solid lines, other interactions are drawn as dashed lines. The lined blocks are used to indicate groups of orbitals that are not discussed here

changes very little as we move from Cl to Br to I. This mirrors the results obtained using the same approach in the case of the trihalides, where the bonding energy of X^- to X_2 varied by less than 1.5 kcal mol^{-1} upon moving along the same series.[5] Another similarity to the trihalides is in the decomposition of the bonding energy. As in those systems, here the net orbital energy term (which we define as the sum of the orbital interaction and Pauli repulsion energies) is repulsive. The bonding energy stems mainly from the electrostatic attraction.

Another interesting point is the magnitude of the preparation energies of the Ph_2IX fragments. For these closed-shell fragments, E_{prep} is defined as the energy required to alter the structure of the fragments from their equilibrium (optimized) geometries to their geometries in the composite molecule. Here E_{prep} is simply the difference between the total bonding energy and the FMO bonding energy. Since the two fragments are identical, the E_{prep} terms in Table 2 can be divided by two to determine the energy required to alter the geometry of each fragment. The largest perturbation of the monomers upon forming the $[Ph_2IX]_2$ dimers is stretching the I—X bond. The magnitude of the stretch varies from 0.29 Å for X = Cl down to 0.22 Å for X = I. These are fairly large geometric perturbations, yet the energies associated with them are quite small (2.3, 2.6 and 2.1 kcal mol^{-1} for X = Cl, Br and I). The potential energy surfaces for stretching the I—X side of the electron-rich three-center Ph—I—X bonds are very flat.

Before delving into the nature of the bonding in these complexes, it is important to note that the net bonding energies

Table 2 Energetics of formation of $[Ph_2IX]_2$ from two Ph_2IX fragments. E_{prep}, the preparation energy, is defined in the text. All energies are in kcal mol^{-1}

	$[Ph_2ICl]_2$	$[Ph_2IBr]_2$	$[Ph_2I_2]_2$
Total bonding energy	−18.3	−16.2	−16.3
FMO bonding energy	−22.6	−21.3	−20.5
Pauli repulsion	61.8	60.3	46.4
Electrostatic attraction	−47.7	−46.2	−37.0
Total orbital energy	−36.7	−35.5	−29.5
E_{prep}	4.6	5.1	4.2

computed are really not very large. When a $[Ph_2IX]_2$ dimer is formed from two Ph_2IX units, two additional I—X bonds are formed. Consequently, the strength of an individual I—X secondary bond is half the total bonding energy for the dimer. This gives an energy of 9.2, 8.1 and 8.2 kcal mol^{-1} per newly formed X—I bond for X = Cl, Br and I, respectively. These energies are quite small, not a great deal larger than those of hydrogen bonds. This reinforces our conclusion that the potential energy surfaces for distorting these molecules (either lengthening the I—X bonds or making them asymmetrical) will be exceedingly flat. Unfortunately, the expense of the calculations prohibits an exploration of this surface.

We have shown that the $[Ph_2IX]_2$ dimers are held together by both electrostatic and donor-acceptor interactions. A reviewer has expressed the result beautifully: 'electrostatic interactions are the engine, donor-acceptor interactions the steering wheel.' Since our previous work demonstrated the equivalence of the donor-acceptor and hypervalent (electron-rich three-center) viewpoints, it is interesting to ask the following question: can we see a relationship between the bonding in these dimers and that in a typical hypervalent compound? Indeed this can be done, but we have to make a few adjustments to take into account the number of atoms and the large bend at the central I. The I—X σ orbitals of $[Ph_2IX]_2$ are shown schematically in Fig. 7. Here we have broken the orbitals into two sets: the first (on the left) utilizes the p_x orbitals on the Xs (these are antisymmetric with respect to the mirror plane through the Xs) and the second (on the right) involves the p_y orbitals on the Xs (symmetric with respect to the mirror plane through the Xs). In both sets of orbitals, we see that the lowest lying orbitals ($9b_{1g}$ and $10b_{2u}$) are I—X bonding, the middle orbitals ($13b_{3u}$ and $14a_{1g}$) are weakly I—X antibonding and the highest orbitals ($13b_{2u}$ and $12b_{1g}$) are strongly I—X antibonding. This hierarchy of bonding is identical to the situation in the standard, linear, electron-rich three-center bonding scheme. Also the same is the occupation of these levels: both sets of three orbitals are occupied through their central member.

The XF_3 monomers

We begin our discussion of the bonding in XF_3 dimers just as we did the discussion of the Ph_2IX dimers above—with the monomers.

The XF_3 monomer geometries were optimized in C_{2v} symmetry; this leaves three geometrical parameters (two bond lengths and one angle) that can be altered. These are illustrated in Scheme 5. The values of these parameters in the optimized geometries of ClF_3, BrF_3 and IF_3, as well as the available gas-phase experimental values, are given in Table 3.

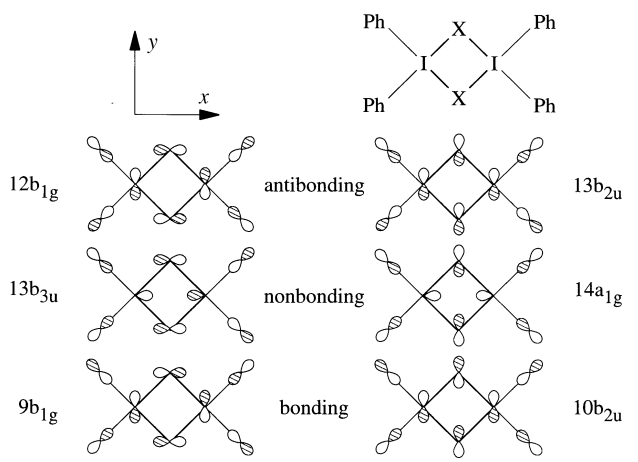

Fig. 7 Iconic representations of some of the frontier orbitals of $[Ph_2IX]_2$

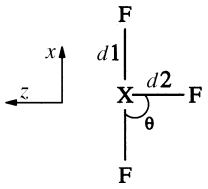

Scheme 5

The optimized geometries match the experimental values fairly well. The calculated bond lengths are all slightly (0.06 Å) too long. Our experience with using ADF to optimize the geometries of halogen-containing species[5] indicates that this overestimation of bond lengths is to be expected. The trends in the angle will be discussed below, after introducing the orbitals of these species.

The energy levels in the frontier orbital region of the XF_3 monomers, along with contour plots of the important MOs of ClF_3, are shown in Fig. 8. The energy level diagrams and frontier MOs of XF_3 bear a striking resemblance to those of Ph_2IX (Fig. 4). This is not surprising, given that the coordination environment of the central halogen in each case is very similar. In both Ph_2IX and XF_3, the central halogen is in a T-shaped coordination environment and is formally in the 3+ oxidation state. The difference is the higher symmetry here: all three ligands around the X are the same.

Table 3 Geometric data for the optimized XF_3 species. All optimizations were carried out in the C_{2v} symmetry. Values in italics are experimental results taken from ref. 15 and 45

	ClF_3		BrF_3		IF_3
*d*1/Å	1.75	*1.70*	1.84	*1.81*	1.97
*d*2/Å	1.66	*1.60*	1.76	*1.72*	1.91
θ/°	89.0	*87.5*	87.2	*82.2*	80.6

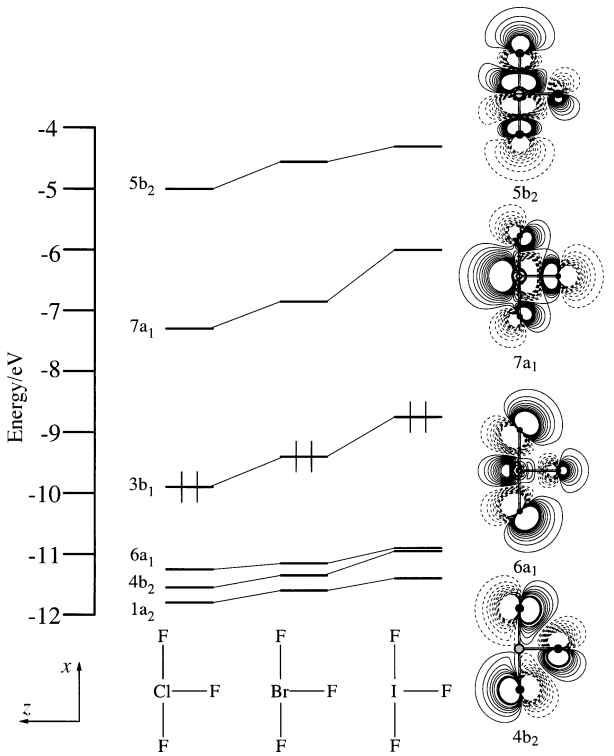

Fig. 8 Energy level diagram in the frontier orbital region for ClF_3, BrF_3 and IF_3. Contour plots in the *xz* plane of the important frontier orbitals of ClF_3 are shown on the right. Orbital $3b_1$, the HOMO, is the completely antibonding combination of p_y orbitals

ClF_3 is a way-point in a series of molecules that begins with PF_5 and SF_4 and ends with XeF_2. The central atom is formally hypervalent with a quasi-linear electron-rich three-center bond. The two highest orbitals in the electron-rich three-center bonding scheme are (in ClF_3) $6a_1$ and $5b_2$; the lowest-lying (completely bonding) member of this set is below the energy window of Fig. 8 at −16.49 eV. The LUMO, $7a_1$, is interesting; it looks at first sight like an unoccupied Cl lone pair orbital, but is to be characterized as mainly the Cl—F σ* orbital.

Within the framework of the Valence Shell Electron Pair Repulsion (VSEPR) model[46] we would expect the X in XF_3, which has three ligands and two lone pairs, to adopt a pseudo-trigonal bipyramidal geometry with the two lone pairs in equatorial positions. Scheme 6 shows these formal lone pairs along with icons of the symmetry-adapted MOs to which they correspond.

Following VSEPR reasoning, because the lone pairs are 'larger' than the electron pairs involved in bonding to the very electronegative F atoms, the two axial F atoms (those along *d*1) should bend back from the lone pairs. This decreases their angle with the equatorial F atom. This is, in fact, what we observe. The bending increases along the series Cl to Br to I with the size of the X atom and, consequently, within the VSEPR scheme the size of the lone pair increases.

Unfortunately, while this straightforward reasoning is qualitatively useful, the actual situation is somewhat more complicated. Each XF_3 monomer has two a_1 symmetry MOs, both of which have X lone pair character. We have already seen one of these orbitals from ClF_3, $6a_1$ in Fig. 8; the other one ($5a_1$) lies lower, below the energy window of Fig. 8 at −12.18 eV. In Fig. 9, which shows these two a_1 orbitals for each of the XF_3 monomers along with the percent contributions of the X atoms, we can see the increase in size of both orbitals with lone pair character upon moving along the series Cl to Br to I. Along this series the contributions of the σ orbital of X to the lone pair MOs increase. At the same time, the amount of X p_z mixed into the lone pair also increases. This admixture of p_z lessens the antibonding interaction with the equatorial F atom by polarizing the lone pair away from it, while at the same time making the lone pair larger.

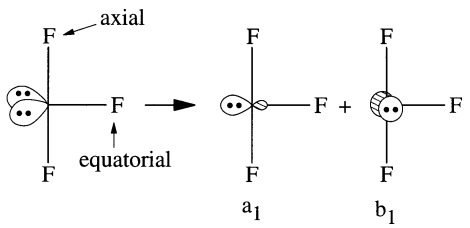

Scheme 6

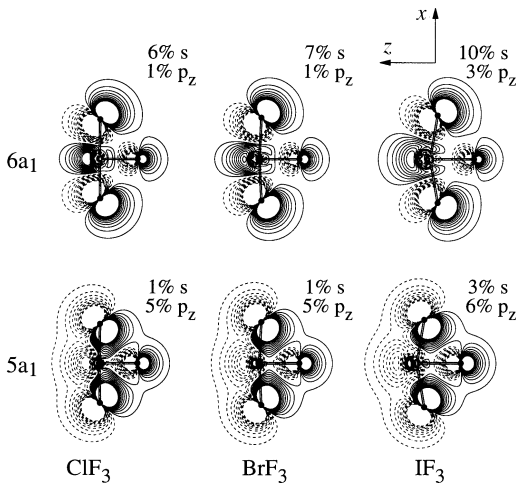

Fig. 9 Contour plots of the two a_1 lone pair orbitals in ClF_3, BrF_3 and IF_3. The numbers above each MO indicate the percent contributions of the σ and p_z AOs on the central X to the MO

Returning to the discussion of Fig. 8, the qualitative trend in the positions of the energy levels of the XF3 species—an upward shift in energy on moving from Cl to Br to I—is understandable in terms of the electronegativity of X. These MOs all have contributions from X, so as the electronegativity of X decreases, the MOs move up in energy.

From the contour plots of Fig. 8 we can see that the XF_3 molecules have orbitals very well-suited to act as donors ($4b_2$ and, to a lesser extent, $6a_1$ in ClF3) and acceptors ($7a_1$, the ClF_3 MO which is maximally antibonding with the F along *d*2). These are the orbitals that will be important in holding the XF_3 dimers together.

The $[XF_3]_2$ dimers

The geometries of the XF_3 dimers were optimized within C_{2h} symmetry. This point group requires that the two XF_3 molecules be equivalent, but allows for an asymmetric dimer. Scheme 7 shows a sketch of the dimer geometry along with definitions of the geometrical parameters. The C_{2h} symmetry allows bonds *d*1 and *d*4 to be of different lengths. However, for X = Cl and X = Br, *d*1 and *d*4 are effectively equal in length in the optimized geometries of the dimers, as may be seen in Table 4. The ClF_3 and BrF_3 dimers optimize to nearly D_{2h} structures, while IF_3 remains C_{2h}. There are no experimental data for gas-phase XF_3 dimers, so we cannot compare our results directly to experiment. Actually, other density functional calculations carried out by one of us (R. M. M.) using different basis sets [6-311 + G(d,p)] and gradient corrections (B3LYP), predict $[ClF_3]_2$ and $[BrF_3]_2$ to be asymmetrical ($d1 \neq d4$). Both sets of computations show (through frequency calculations) the calculated geometries to be true minima on potential energy surfaces that are very flat. For instance, a D_{2h} $[IF_3]_2$ (see Table 4) is only 2.7 kcal mol^{-1} above our calculated minimum.

Given the energetic flatness of the underlying surface, the conflict between these two sets of results will not be discussed here. As it turns out, since we are not interested here in studying the degenerate fluorine transfer reaction between XF_3 molecules,[47] these differences are not especially important to the discussion that follows. There is strong agreement between

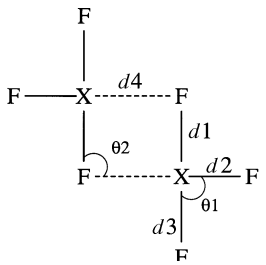

Scheme 7

Table 4 Geometric data for the optimized $[XF_3]_2$ species. All optimizations were carried out in the C_{2h} symmetry except for the second $[IF_3]_2$ geometry, which was optimized in D_{2h}, as explained in the text

	$[ClF_3]_2$	$[BrF_3]_2$	$[IF_3]_2$	$[IF_3]_2$ D_{2h}
*d*1/Å	2.05	2.14	2.07	2.27
*d*2/Å	1.70	1.80	1.96	1.94
*d*3/Å	1.70	1.80	1.91	1.94
*d*4/Å	2.05	2.14	2.52	2.27
θ1/°	94.2	94.1	83.3	92.5
θ2/°	97.4	99.9	111.7	101.9

the two sets of computed dimer bonding energies, and this is the quantity upon which we will be focusing.

To facilitate comparison with the other results, $[IF_3]_2$ was also optimized within the D_{2h} symmetry. The geometry of this structure is also reported in Table 4. In the rest of this analysis, we will focus our attention on the D_{2h} geometry of $[IF_3]_2$.

Within the symmetrical dimers ($[ClF_3]_2$, $[BrF_3]_2$ and $[IF_3]_2$ D_{2h}) the $d1$ bonds, those involved in the bridging, are stretched an almost constant amount (0.30 Å) relative to their lengths in the optimized monomers. Bonds $d2$, which are opposite the bridge, are also slightly stretched (0.04 Å). These results are to be expected if the donor-acceptor interaction leads to partial occupation of orbital $7a_1$ (Fig. 8), which is antibonding between the X and F atoms.

An FMO diagram for the interaction of two ClF_3 fragments to form $[ClF_3]_2$ is shown in Fig. 10. We can see, as was the case for $[Ph_2ICl]_2$ (Fig. 6), that the acceptor orbital of a monomer ($7a_1$ here) is mixed into the populated states. The calculated occupation of this orbital in the symmetric dimers is 0.34, 0.30 and 0.23 for $[ClF_3]_2$, $[BrF_3]_2$ and $[IF_3]_2$ D_{2h}, respectively. The donor orbital of the monomer ($4b_2$) is mixed into unpopulated orbitals of the complementary fragment, giving $4b_2$ occupations of 1.72, 1.75 and 1.87 in the three dimers. In contrast to the $[Ph_2IX]_2$ story, there is donation from another orbital as well in these XF_3 dimers. MO $6a_1$ (the lone pair orbital) is also slightly depopulated, with occupations of 1.91, 1.90 and 1.88 in $[ClF_3]_2$, $[BrF_3]_2$ and $[IF_3]_2$ D_{2h}. There are no significant stabilizing interactions within the fully occupied (and thus antibonding) π system of the dimer.

The energy decomposition for the XF_3 dimers is shown in Table 5. As was the case in the trihalides and the Ph_2IX dimers discussed above, the net orbital energy (the sum of the Pauli and orbital interaction terms) is destabilizing. Using this partitioning scheme, the majority of the bonding energy arises from the electrostatic term. Though the FMO bonding energies here are significantly larger than those in the Ph_2IX dimers (Table 2), the total bonding energies are quite a bit smaller. The big difference is the magnitude of the preparation energy required to distort the XF_3 fragments to their geometries in the dimers. The distortions of the monomers are only slightly larger than they were in the Ph_2IX dimers, but these distortions cost considerably more energy. The potential energy surfaces for distortions of the XF_3 monomers are not nearly as flat as they were for the Ph_2IX species.

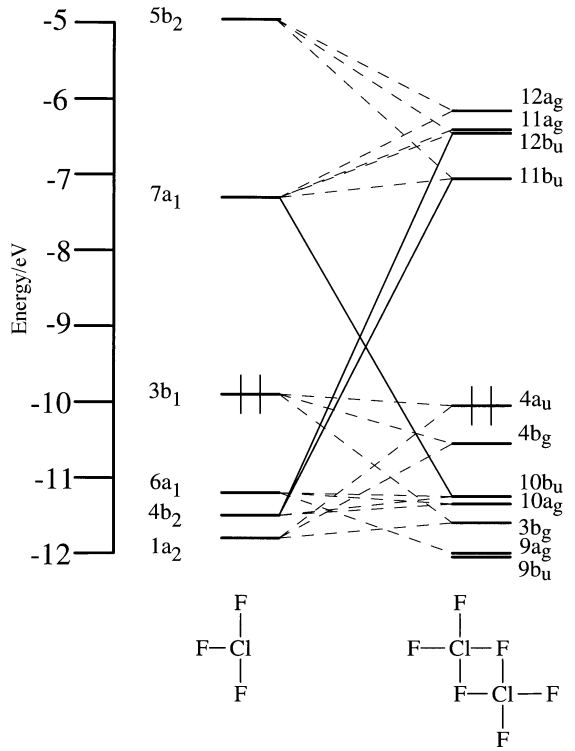

Fig. 10 FMO interaction diagram for the formation of $[ClF_3]_2$ from two ClF_3 fragments. Interactions involved in the donor-acceptor interaction are drawn with solid lines, other interactions are drawn as dashed lines

Table 5 Energetics of formation of $[XF_3]_2$ from two XF_3 fragments. All energies are in kcal mol^{-1}

	$[ClF_3]_2$	$[BrF_3]_2$	$[IF_3]_2$ D_{2h}
Total bonding energy	−9.0	−11.1	−5.2
FMO bonding energy	−34.2	−37.1	−34.1
Pauli repulsion	120.7	123.1	129.1
Electrostatic attraction	−66.1	−74.8	−86.8
Total orbital energy	−88.9	−85.3	−76.5
E_{prep}	25.2	26.0	28.9

The bridging X—F bond energies in these XF_3 dimers (calculated the same way as the I—X bonding energy in $[Ph_2IX]_2$ above: by dividing the total bonding energy by two): 4.5, 5.6 and 2.6 kcal mol^{-1} for X = Cl, Br and I, are quite small. The increase in the FMO bonding energies relative to those in the $[Ph_2IX]_2$ dimers is offset to a large extent by the larger preparation energies of the XF_3 fragments. So, while the intermolecular interactions involving bridging F atoms are stronger than those using the other halogens (as measured by the FMO bonding energy), the cost of stretching the X—F bonds makes the net interaction (including E_{prep}) weaker.

As might be expected based upon all the other similarities, the frontier orbitals of the XF_3 dimers (not shown) look a lot like those of $[Ph_2ICl]_2$. It is once again possible to interpret the shapes of the MOs of these donor-acceptor complexes quite cleanly in terms of the modified electron-rich three-center bonding scheme shown in Fig. 7.

Conclusions

Our analysis shows that the halogen—halogen secondary bonding that holds both Ph_2IX and XF_3 dimers together is easily understood in terms of either donor-acceptor interactions between the monomers or a modified electron-rich three-center bonding model. These interactions are relatively weak; the secondary bonds themselves are worth less than 10 kcal mol^{-1}. In both families of compounds, the FMO bonding energies and preparation energies are similar in size. As was the case in the trihalides, the FMO bonding energy in these systems is dominated by the electrostatic term in the transition state energy decomposition procedure; the total orbital interaction between these neutral, closed-shell species is destabilizing. Because the potential energy surface for distortions of the dimers is very flat, crystal packing forces are likely to give a range of dimer geometries: both distorted and nearly symmetrical, in the solid state.

We can further apply the donor-acceptor model that we have developed here to the intermolecular interactions shown schematically in Scheme 2. In Scheme 8 these coordination geometries are reproduced, along with icons of the orbitals involved in the interactions. When an electrophile (an

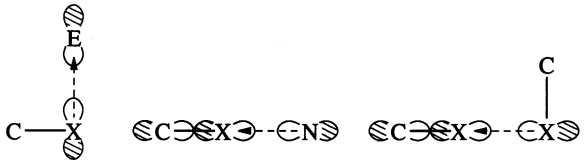

Scheme 8

acceptor) approaches a C—X bond (left side in Scheme 8), it accepts electrons from the Cl lone pairs that are perpendicular to the C—X bond. When a nucleophile (a donor) coordinates (center in Scheme 8), it does so by transferring electrons into the C—X σ* orbital. Consequently, the nucleophile must approach parallel to the C—X bond. Finally, interaction between two C—X units (right side in Scheme 8) occurs in such a way that the X-centered lone pair of one C—X bond is oriented towards the C—X σ* level of the other. These conclusions are in agreement with the structural sytematics found in a previous study[19].

A reviewer has remarked that there is a structural relationship between the dimers studied here and binuclear d^8 transition metal ions with the general formula $[L_2M(\text{-}X)_2ML_2]$, which are frequently nonplanar.[48]

Acknowledgements

G. A. L., N. G., and R. H. are grateful to the National Science Foundation for its support of their work through Research Grant CHE 94-08455. They would also like to thank Silicon Graphics for their generous donation of the computer hardware which was used in a portion of this work. A portion of the research was conducted using the resources of the Cornell Theory Center, which receives major funding from the NSF and New York State, with additional support from the Advanced Research Projects Agency (ARPA), the National Center for Research Resources at the National Institutes of Health (NIH), IBM Corporation, and other members of the center's Corporate Partnership Program.

R. M. M. thanks the Cherry L. Emerson Center for Scientific Computation at Emory University for a fellowship and the Russian Fund for Basic Research for financial support of this work.

References

1 N. W. Alcock, *Adv. Inorg. Radiochem.*, 1972, **15**, 1.
2 M. Trömel, in *Unkonventionelle Wechselwirkungen in der Chemie metallischer Elemente*, ed. B. Krebs, VCH, Weinheim, 1992, ch. 6.
3 I. Haiduc, *Coord. Chem. Rev.*, 1997, **158**, 325.
4 I. Haiduc, R. B. King and M. G. Newton, *Chem. Rev.*, 1994, **94**, 301.
5 G. A. Landrum, N. Goldberg and R. Hoffmann, *J. Chem. Soc., Dalton Trans.*, 1997, 3605.
6 G. C. Pimentel, *J. Chem. Phys.*, 1951, **19**, 446.
7 R. E. Rundle, *J. Am. Chem. Soc.*, 1979, **101**, 5057.
8 P. Pyykkö, *Chem. Rev.*, 1997, **97**, 597.
9 N. W. Alcock and R. M. Countryman, *J. Chem. Soc., Dalton Trans.*, 1977, 217.
10 P. J. Stang and V. V. Zhdankin, *Chem. Rev.*, 1996, **96**, 1123.
11 G. F. Koser, in *The Chemistry of Halides, Pseudo-halides and Azides*, ed. S. Patai and Z. Rappaport, Wiley, New York, 1995, ch. 21.
12 A. Varvoglis, *Hypervalent Iodine in Organic Synthesis*, Academic Press, New York, 1997.
13 H. Schmitz and H. J. Schumacher, *Z. Naturforsch., A*, 1947, **2**, 363.
14 M. Rogers, H. B. Thompson and J. L. Speirs, *J. Am. Chem. Soc.*, 1947, **76**, 4841.
15 R. A. Frey, R. L. Redington and A. L. K. Aljibury, *J. Chem. Phys.*, 1971, **54**, 344.
16 R. D. Burnank and F. N. Bensey, *J. Chem. Phys.*, 1953, **21**, 602.
17 A. M. Ellern, M. Y. Antipin, Y. T. Struchkov and V. F. Sukhoverkhov, *Russ. J. Inorg. Chem.*, (Engl. Transl.), 1991, **36**, 792.
18 P. Schwerdtfeger, *J. Phys. Chem.*, 1996, **100**, 2969.
19 N. Ramasubbu, R. Parthasarathy and P. Murray-Rust, *J. Am. Chem. Soc.*, 1986, **108**, 4308.
20 S. E. Novick, K. C. Janda and W. Klemperer, *J. Chem. Phys.*, 1976, **65**, 5115.
21 F. A. Baiocchi, T. A. Dixon and W. Klemperer, *J. Chem. Phys.*, 1982, **77**, 1632.
22 N. N. Greenwood and A. Earnshaw, *Chemistry of the Elements*, Pergamon Press, New York, 1984.
23 S. L. Price, A. J. Stone, J. Lucas, R. S. Rowland and A. E. Thornley, *J. Am. Chem. Soc.*, 1994, **116**, 4910.
24 J. P. Lommerse, A. J. Stone, R. Taylor and F. H. Allen, *J. Am. Chem. Soc.*, 1996, **118**, 3108.
25 S. C. Nyburg and W. Wong-Ng, *Proc. R. Soc. London A*, 1979, **367**, 29.
26 V. G. Tsirelson, P. F. Zou, T. H. Tang and R. F. W. Bader, *Acta Crystallogr., Sect. A*, 1995, **51**, 143.
27 E. J. Baerends, D. E. Ellis and P. Ros, *Chem. Phys.*, 1973, **2**, 41.
28 E. J. Baerends and P. Ros, *Chem. Phys.*, 1975, **8**, 412.
29 E. J. Baerends and P. Ros, *Int. J. Quantum Chem. Symp.*, 1978, **12**, 169.
30 A. D. Becke, *J. Chem. Phys.*, 1986, **84**, 4524.
31 A. D. Becke, *Phys. Rev. A*, 1988, **38**, 3098.
32 J. P. Perdew, *Phys. Rev. B*, 1986, **33**, 8822.
33 J. P. Perdew, *Phys. Rev. B*, 1986, **34**, 7406.
34 J. G. Snijders, E. J. Baerends and P. Vernoojis, *At. Nucl. Data Tables*, 1982, **26**, 483.
35 C. Lee, W. Yang and R. G. Parr, *Phys. Rev. B*, 1988, **37**, 785.
36 B. G. Johnson, P. M. W. Gill and J. A. Pople, *J. Chem. Phys.*, 1993, **98**, 5612.
37 T. V. Russo, R. L. Martin and P. J. Hay, *J. Chem. Phys.*, 1994, **101**, 7729.
38 G. A. Landrum, YAeHMOP is freely available on the World Wide Web at URL: http://overlap.chem.cornell.edu:8080/yaehmop.html, 1995.
39 T. Ziegler, in *Metal-ligand Interactions: from Atoms, to Clusters, to Surfaces*, ed. D. R. Salahub and N. Russo, Kluwer Academic, Amsterdam, 1992, p. 367.
40 H. Ikezawa, M. Takahashi, M. Takeda and Y. Ito, *Bull. Chem. Soc. Jpn.*, 1993, **66**, 1959.
41 It is important to remember that there is no direct correlation between the orbital energies from the density functional calculation and any experimentally measureable quantity, such as ionization potential. R. G. Parr, and W. Yang, *Density-Functional Theory of Atoms and Molecules*, Oxford University Press, New York, 1989.
42 Owing to their low symmetry, there is no strict σ-π separability in these molecules, we use the labels as a notational convenience to distinguish p orbitals that are parallel or perpendicular to the I—X axis.
43 Hirshfeld analysis was used to calculate charges due to the well-known failings of the standard Mulliken analysis when large basis sets are used in a calculation. F. L. Hirshfeld, *Theor. Chim. Acta*, 1977, **44**, 129.
44 R. J. Hach and R. E. Rundle, *J. Am. Chem. Soc.*, 1951, **73**, 4321.
45 D. F. Smith, *J. Chem. Phys.*, 1953, **21**, 609.
46 R. J. Gillespie and E. A. Robinson, *Angew. Chem. Int. Ed. Engl.*, 1996, **35**, 495.
47 A computational study of this reaction is being carried out by one of us (R. M. M.).
48 (*a*) R. H. Summerville and R. Hoffmann, *J. Am. Chem. Soc.*, 1976, **98**, 7240 and references therein. (*b*) P. Alemany and S. Alvarez, *Inorg. Chem.*, 1992, **31**, 4266. (*c*) G. Aullón, P. Alemany and S. Alvarez, *J. Organomet. Chem.*, 1994, **75**, 478. (*d*) C. Mealli and A. Orlandini, to be published.

Received in Montpellier, France 28th January, 1998;
Paper 8/00910D